SIMULATIONS AND MEASUREMENTS OF THE PRE-ARCING TIMES IN HBC FUSES UNDER TYPICAL ELECTRIC FAULTS

Steeve Sm Memiaghe, David Rochette, Rachid Touzani, Pascal André

SIMULATIONS AND MEASUREMENTS OF THE PRE-ARCING TIMES IN HBC FUSES UNDER TYPICAL ELECTRIC FAULTS

S. Memiaghe [1,3*], W. Bussière [1,3], D. Rochette [1,3], R. Touzani [2,3] and P. André [1,3]

[1] *Laboratoire Arc Electrique et Plasmas Thermiques CNRS FRE 3120, Phys. Bât. 5 - Université Blaise Pascal 24, Avenue des Landais 63177 Aubière Cedex, France*
[2] *Laboratoire de Mathématiques CNRS UMR 6620, Campus Universitaire des Cézeaux, 24 Avenue des Landais, F63177 Aubière Cedex, France*
[3] *P.R.E.S. Clermont Université, 9 rue Kessler B.P. 10448 63012 Clermont-Ferrand Cedex 1.*
*steeve.memiaghe@univ-bpclermont.fr

Abstract

This work deals with the comparison between calculations and measurements of pre-arcing times in High Breaking Capacity fuses under typical fault current conditions. This paper also describes the temperature evolution and the Joule energy dissipated in a fuse element during the pre-arcing time. By varying typical electrical parameters, namely the closing angle and the power factor, we show that various prospective currents such as those observed in industrial case can be fairly simulated. The pre-arcing time and then the clearing of the fault current are shown to be deeply dependent on these electrical characteristics. We exhibit simulated results of prospective current and supply voltage waves for given closing angles under two typical power factors which are compared with the experimental ones. A comparison between simulated pre-arcing times with experimental ones shows some discrepancies and a discussion on the numerical assumptions is made.

Keywords
HBC fuses; pre-arcing time; closing angle; power factor; prospective current.

1. INTRODUCTION

The role of High Breaking Capacity (HBC) fuses is to restrict the damages to the persons and to the electrical equipments by limiting and interrupting prospective faults occurring in power distribution networks and in industrial installations. This is realized by means of the combination of four main elements from which HBC fuses are built. A typical HBC fuse consists of a calibrated silver fuse element. This fuse element configuration (geometry and notches regularly spaced through the length) and its physical properties (resistance for example) are selected to achieve a good conducting current path through the fuse. The current path is also ensured by fuse contacts (in each end side of the fuse) in which the fuse element is welded. The fuse element is surrounded by silica sand as filler which role is to absorb the heat generated by the fuse element and to absorb the arc energy when the fuse clears the fault current. The fuse element and the filler are enclosed in a mechanically and thermally strengthened cylindrical fuse body. When a sustained overload occurs, the fuse element will generate heat (especially in the notches) dissipated along the fuse length in a first time, and in a second time the heat can be passed to the filler. If the overload persists and becomes higher, the thermal equilibrium is not achieved in the fuse, and then the fuse element reaches firstly

its melting point, secondly its vaporization point and finally disrupts by the appearance of an electric arc [1]. Industrialists call this time step the pre-arcing time. The electric arc created leads to a silver plasma composed of metallic vapours. When increasing its length (burn-back phenomenon), the electric arc also interacts with the sand filler due to the energy brought by the fault. Once the electric arc is much longer, this latter could not be maintained by the supply voltage and then the current in the fuse falls to zero. This defines the arcing time. The whole fuse operation is usually divided in these two latter stages [1].
In the past many authors were interested in the optimization of fuse performance with special reference to the pre-arcing. Some studies were carried out under *AC* supply [2-6], others under *DC* supply [2,5]. The main tasks of these investigations were to understand in which manner electrical characteristics of a circuit network play a role in the fuse performance and to link the electrical energy dissipation of the fuse to the prediction of pre-arcing times.
In this work the pre-arcing behaviour of HBC fuses is analysed in the case of realistic industrial test conditions in terms of some characteristics of the prospective fault current under *AC* supply. This is done by varying the closing angle and the power factor values founded in industrial HBC fuses. As the closing angle and the power factor values decide respectively on the instant of appearance and on the magnitude of the fault, the pre-arcing time is strongly dependent on their values. Simulations and measurements are carried out for closing angle values varying in a wide range as in industrial operation and for two power factor values corresponding to the two typical cases namely the inductive case and the resistive case. In section 2, the experimental test is presented, following by the geometry of the fused element used in simulation and in experiments and the mathematical model. The simulated and experimental results are exhibited in section 3 and discussion is drawn on in section 4. Conclusion is done after.

2. EXPERIMENTAL SET UP AND THERMO-ELECTRICAL MODEL

2.1 Experimental test

The experimental test device built from a 100kVA true single-phase transformer has been designed to reproduce the whole fuse operation in fault conditions similar to the industrial test conditions. The experimental device and the test operation have been described in previous works by Bussière *et al* [6] and Memiaghe *et al* [7]. The main electrical parameters of the measurements are recalled hereafter.

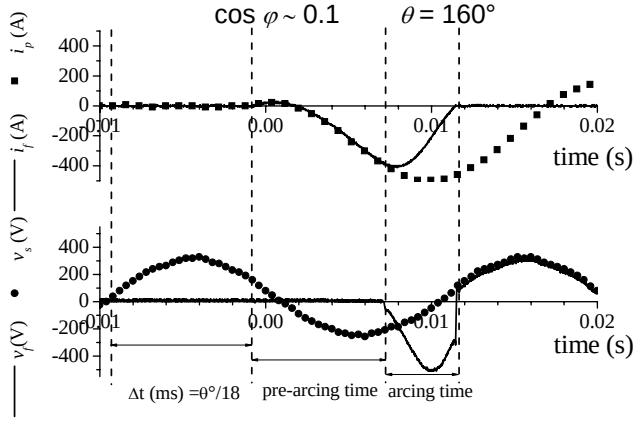

Figure 1 : Characteristic curves of fuse breaking under *AC* supply: fuse voltage v_f, supply voltage v_s, fuse current i_f, prospective current i_p.

The first step before a fuse operation is to set the closing angle (defined as the phase angle of the beginning of the fault current or prospective current i_p once the supplied voltage v_s is applied to the fuse) and the power factor. The closing angle θ is expressed in time units (figure 1) by:

$$\Delta t(ms) = \frac{\theta(^\circ)}{18} \tag{1}$$

The power factor is deduced from the following formula:

$$\cos\varphi = \frac{R}{\sqrt{R^2 + L^2\omega^2}} \tag{2}$$

where R and L are respectively the resistive load and the inductive load, ω is the pulsation calculated at 50 Hz.

The second step is to set the prospective current which stands for the electric fault. This fault is calculated as:

$$i_p(t) = \frac{\hat{V}}{\sqrt{(R^2 + L^2\omega^2)}} \times \left(\sin(\omega t + \theta - \varphi) - \sin(\theta - \varphi) \times e^{-\frac{R}{L}t} \right) \tag{3}$$

where $\hat{V}$ is the peak value of the supply voltage at 50 Hz and t is the time. It is important to notice that according to international standards [8], the current passing through the fuse is equated to the prospective fault current during the whole pre-arcing stage. So current $i_p(t)$, current $i_f(t)$ and current $i(t)$ stand for the same fuse current.

The Joule energy W_J dissipated in the fuse-link due to the passage of the fault current during the pre-arcing time (duration t_p) is given by:

$$W_J = \int_0^{t_p} R_f(t) \times i^2(t) dt\,, \tag{4}$$

where R_f is the fuse resistance.

2.2 Fuse element geometry

Simulations and experiments have been carried out for a fuse-link with circular reduced section shape of $l' \times e = 0.5 \times 0.105$ mm^2. The fuse-link length is L=66 mm and its cross-section area is $l \times e = 1 \times 0.105$ mm^2. For the experiments, the fuse element (designed to reproduce elementary phenomenon occurring in industrial fuses) is introduced in the circuit network by means of an experimental fuse cell as depicted in [6].

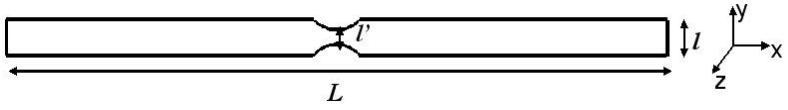

Figure 2 : Fuse element geometry used in simulations and experiments.

2.3 Thermo-electrical model

The mathematical model dealt with thermal effect and electrical effect problem. This problem is based on the heat transfer equation with conduction as the main heat loss term and Joule heating as the main source term. The thermo-electrical problem is usually written as:

$$\frac{\partial H}{\partial t} - \nabla.(k_{Ag} \nabla T) = \frac{|\mathbf{J}|^2}{\sigma_{Ag}}, \tag{5}$$

where H represents the enthalpy of the silver fuse-link, k_{Ag} and σ_{Ag} are respectively the thermal and the electrical conductivity of silver (both depending on enthalpy) and $\boldsymbol{J}$ is the

current density vector. The current density is obtained from the Laplace equation and the Ohm's law which are governed by:

$$\nabla.(\sigma_{Ag}\nabla V) = 0,$$
$$\mathbf{E} = -\nabla V, \qquad (6)$$
$$\mathbf{J} = \sigma_{Ag}\mathbf{E}.$$

V is the potential and $\boldsymbol{E}$ is the electric field vector. To solve numerically the system (Eq.5 – Eq.6), the finite elements *method* is used for space discretization and a *Chernoff scheme* is used for time integration. Details of the mathematical model and the numerical method are reported in Rochette *et al* [9].

3. RESULTS

We present results of prospective current, supply voltage and the temperature evolutions during the pre-arcing stage under given power factor and closing angle.

3.1 Closing angle of θ=12.1 under inductive power factor cos φ ~ 0.1

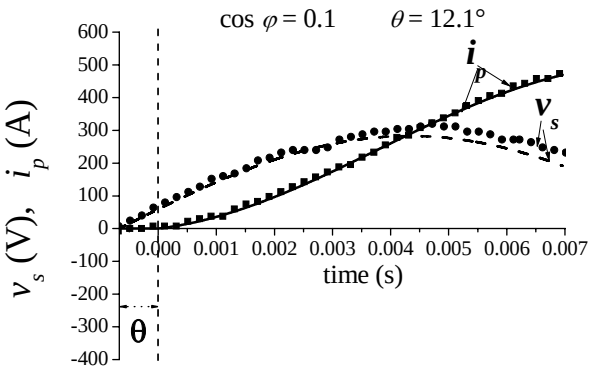

Figure 3 : Simulated (line) and measured (full squares) prospective fault i_p and simulated (dash) and measured (full circles) supply voltage v_s during the pre-arcing time.

Figure 3 presents the simulated and the experimental waveforms of the prospective current i_p and the supply voltage v_s during the pre-arcing time in the case of a power factor fixed at $\cos\varphi \sim 0.1$ and a closing angle of θ=12.1°. In simulation the pre-arcing time is obtained once the whole latent heat of vaporization is provided. This simulated pre-arcing time is 6.96 ms and the pre-arcing time measured is 6.13 ms (the relative discrepancy is about 12%).

In Figure 4 is exhibited the simulated fuse-link temperature rise and the Joule energy W_J dissipated in the fuse during the pre-arcing time. W_J at the end of pre-arcing time is 10.80 J. We give also the temperature T_{eq} corresponding to the pre-arcing time measured. The pre-arcing time measured is reported on the simulated temperature curve to estimate a temperature related to the pre-arcing time obtained in experiments. This temperature is T_{eq} *=1656 K*. The temperature evolution exhibits four main stages. During the first stage 1 W_J is devoted to rise the temperature of the fuse element from its initial temperature (300 K) up to its melting temperature (T_m). During the second stage 2 W_J is involved in the solid to liquid state change by means of the latent heat of fusion. This state change participates in a considerable variation of the fuse-link resistivity (the ratio of the liquid resistivity to the solid resistivity for silver is about ~2.1 [10]) and consequently the liquid resistivity leads to a fast temperature rise up to the vaporization temperature (T_v) as it can be seen in the third stage 3. In the fourth stage 4, the constant fuse-link temperature observed is due to the latent heat of vaporization which

requires a significant energy (about 10 times related to the energy necessary for the latent heat of fusion [11]) is necessary for the whole liquid-vapour state change.

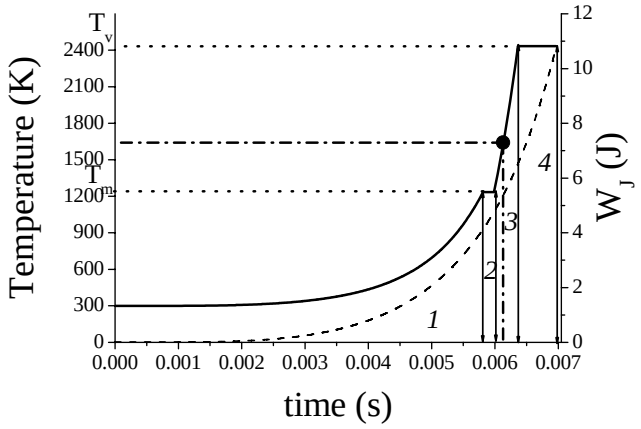

Figure 4: Simulation of the temperature evolution (continuous line) with the experimental value of t_p (solid circle) and W_J (dashed line) in the fuse during the pre-arcing time.

3.2 Closing angle of θ=90° under inductive power factor cos φ ~ 0.1

Figure 5 gives the waveforms of i_p and v_s during the pre-arcing time in the case of cos φ ~ 0.1 and for θ=90° for simulation and experiments. Simulation and experiments give respectively pre-arcing times of 14.16 ms and 12.68 ms (the relative discrepancy is about 10%). The limitation of the fault current occurs in the second half-wave and the pre-arcing time is in both cases much longer compared to the previous ones obtained for θ = 12.1°.

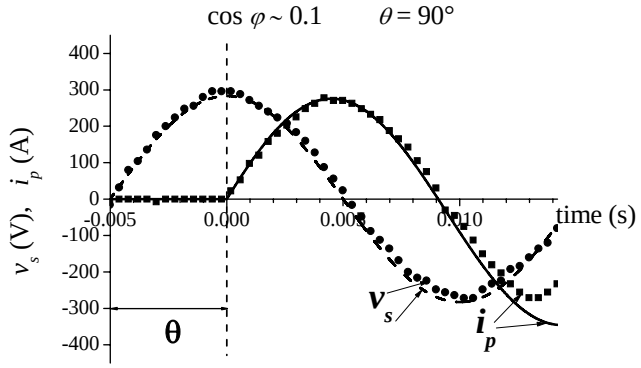

Figure 5: Simulated (line) and measured (full squares) i_p and simulated (dash) and measured (full circles) v_s during the pre-arcing time.

This result is interesting because the fault current has two main characteristics that the fuse tends to reduce as better as possible: the duration and the magnitude. The duration and the magnitude of the fault are expressed in a parameter which characterizes all fuse performances, the *Joule integral* ($I^2t = \int_0^{tp} i^2(t)dt$). These two characteristics are significant in the case of θ = 90° because in this case the Joule energy is maximum.

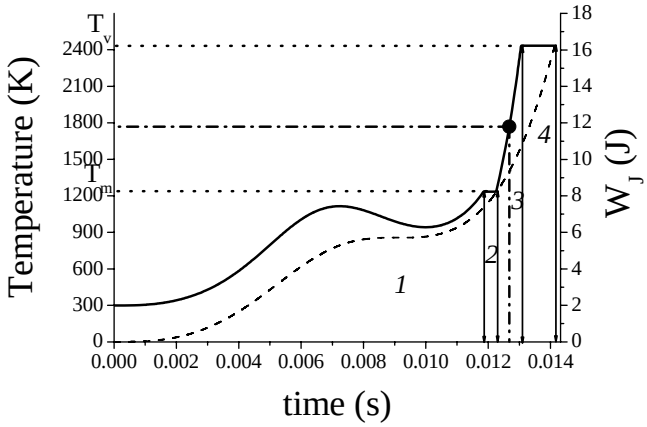

Figure 6: Simulation of the temperature evolution (continuous line) with the experimental value of t_p (solid circle) and W_J (dashed line) in the fuse during the pre-arcing time.

This is illustrated in figure 6 which exhibits the temperature and the W_J plotted as a function of the time. W_J at the end of pre-arcing is 16.45 J and is 65% higher than that of θ=12.1°. An estimate of temperature corresponding to the pre-arcing time measured is T_{eq} =1766 K.
The curve of figure 6 presents the four main evolutions as it was seen in figure 4. In stage 1 of figure 6 the fuse temperature increases and decreases due to the current waveform. This means that once the current falls down and reaches zero, the Joule heating also decreases: heat transfer by conduction from the hottest points of the fuse element to the remainder fuse appears and consequently the temperature decreases.

3.3 Closing angle of θ=160° under inductive power factor cos φ~0.1

In figure 7 we show the prospective current and the supplied voltage waveforms for a closing angle of *160°* both for simulations and experiments in the case of cos $\varphi \sim$ 0.1. From the appearance up to the passage to zero in the first half-cycle, the fault current could not really damages the fuse due to the fact that the magnitude of the fault is not significant ($i_{p,peak}$ ~19 A) during this period.

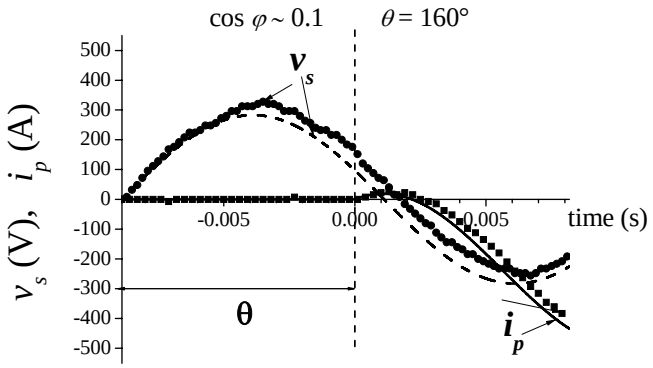

Figure 7: Simulated (line) and measured (full squares) i_p and simulated (dash) and measured (full circles) v_s during the pre-arcing time.

The current limitation occurs in the second half-wave and the pre-arcing time is 8.85 ms for simulations and 7.90 ms for experiments. The relative discrepancy is about 11%.

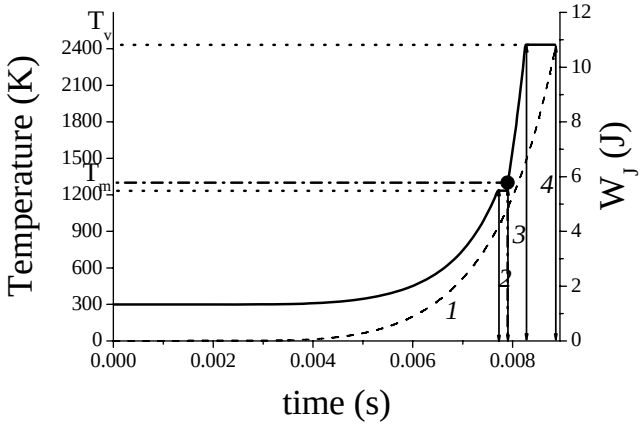

Figure 8: Simulation of the temperature evolution (continuous line) with the experimental value of t_p (solid circle) and W_J (dashed line) in the fuse during the pre-arcing time.

Figure 8 shows the temperature and the Joule energy histories during the pre-arcing time. W_J at the end of pre-arcing time is 10.67 J. From the energy point of view the characteristics of figure 8 are very similar to those obtained in the case of θ=12.1° of which W_J is 10.80 J. The duration of the fault current in the first half-cycle (about 2 ms) for θ=160° explains the difference between pre-arcing times values. Figure 8 also gives the estimated temperature corresponding to the pre-arcing time obtained in experiments which is T_{eq} =1300 K.

3.4 Closing angle of θ=6.7° under resistive power factor cos φ ~ 0.9

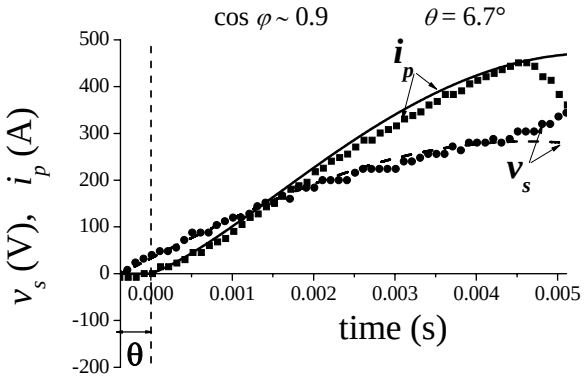

Figure 9: Simulated (line) and measured (full squares) prospective current i_p and simulated (dash) and measured (full circles) v_s during the pre-arcing time.

Figure 9 presents the waveforms of the prospective current i_p and the supply voltage v_s during the pre-arcing time in the case of *cos* φ ~ 0.9 and for θ=6.7° for simulations and experiments. Simulations and experiments give respectively pre-arcing times of 5.11 ms and 4.67 ms (the relative discrepancy is about 9%). Compared to the simulated pre-arcing time obtained in the case of cos φ ~ 0.1 for θ=12.1°, the pre-arcing time obtained from simulations in this case, is shorter and the relative difference represents about 27%. The same observation is done when looking to the measured pre-arcing times for which the difference is about 24%. The value of the closing angle is not the main reason to explain this difference; but the magnitude of the fault current which is higher in the resistive case compared to the inductive one.

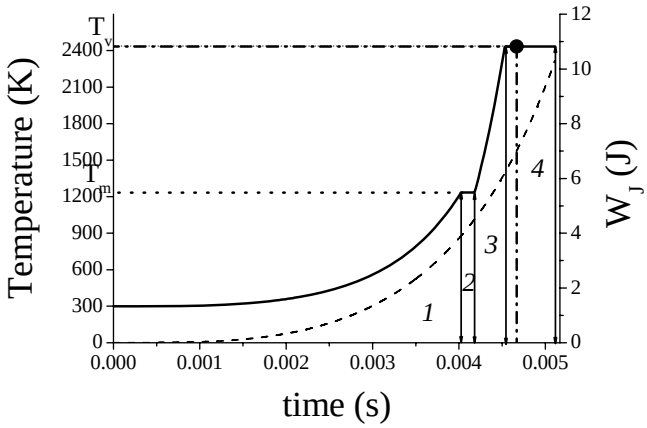

Figure 10: Simulation of the temperature evolution (continuous line) with the experimental value of t_p (solid circle) and W_J (dashed line) in the fuse during the pre-arcing time.

Figure 10 shows the temperature and the dissipated energy histories during the pre-arcing time. W_J at the end of pre-arcing time is 10.30 J is quite equal than to that obtained in the case of cos $\varphi \sim 0.1$ for θ=12.1°. Figure 8 also gives the estimated temperature corresponding to the pre-arcing time obtained in experiments which given by T_{eq} = 2433 K.

3.5 Closing angle of θ=90° under resistive power factor cos $\varphi \sim 0.9$

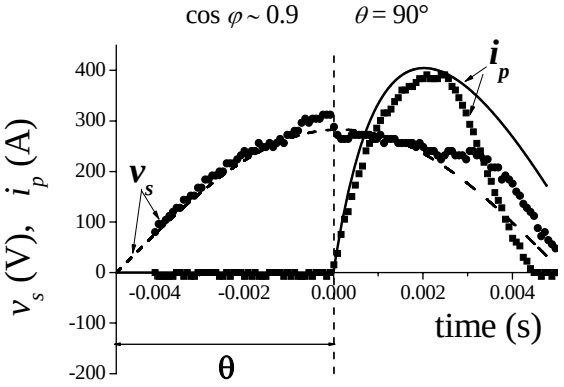

Figure 11: Simulated (line) and measured (full squares) i_p and simulated (dash) and measured (full circles) v_s during the pre-arcing time.

Figure 11 presents the waveforms of the prospective current i_p and the supply voltage v_s during the pre-arcing time in the case of cos $\varphi \sim$ 0.9 and for θ=90° for simulation and experiments. Simulations and experiments give respectively pre-arcing times of 4.77 ms and 2.53 ms (the relative discrepancy is about 47%).

Figure 12 shows the temperature and the Joule energy histories during the pre-arcing time. W_J at the end of pre-arcing time is 10.48 J and the estimated temperature corresponding to the pre-arcing time obtained in experiments which correspond to T_{eq} = *1235 K.*

3.6 Closing angle of θ=160° under resistive power factor cos $\varphi \sim 0.9$

Figure 13 presents the waveforms of the prospective current i_p and the supply voltage v_s during the pre-arcing time in the case of cos $\varphi \sim$ 0.9 and for θ=160° for simulation and

experiments. Simulations and experiments give respectively pre-arcing times of 6.60 ms and 5.64 ms (the relative discrepancy is about 15%).

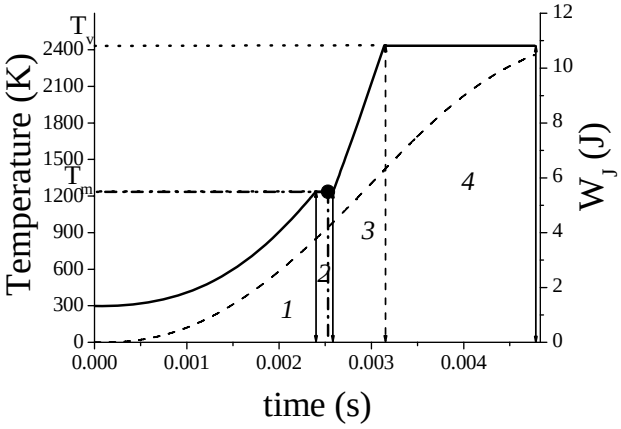

Figure 12: Simulation of the temperature evolution (continuous line) with the experimental value of t_p (solid circle) and W_J (dashed line) in the fuse during the pre-arcing time.

Figure 14 shows the temperature and the Joule energy histories during the pre-arcing time. W_J at the end of pre-arcing time is 10.37 J and the estimated temperature corresponding to the pre-arcing time obtained in experiments which correspond to $T_{eq} = 1235$ *K*.

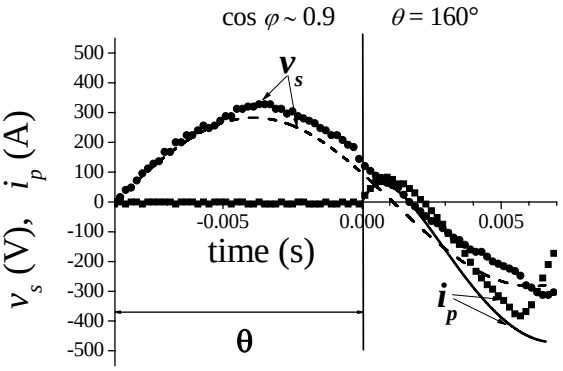

Figure 13: Simulated (line) and measured (full squares) i_p and the simulated (dash) and measured (full circles) v_s during the pre-arcing time.

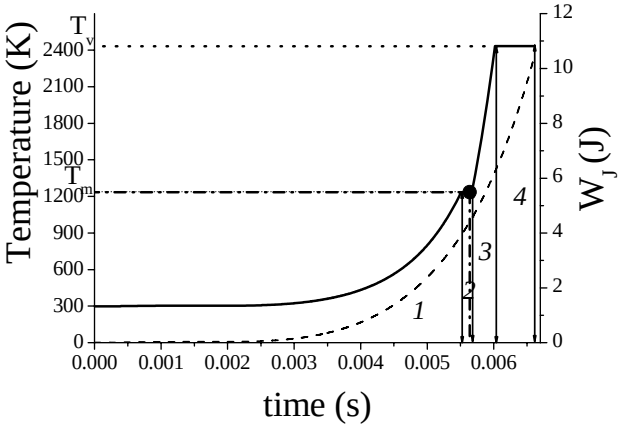

Figure 14: Simulation of the temperature evolution (continuous line) with the experimental value of t_p (solid circle) and W_J (dashed line) in the fuse during the pre-arcing time.

3.7 Summary of the results

In table 1, we recall the different pre-arcing time values obtained from simulation and experiment with the discrepancies observed. In table 2 a reminder of the corresponding temperature of measured pre-arcing time is given.

Table 1: Relative discrepancy between simulated and experimental pre-arcing times.

	Simulations	Experiments	Relative discrepancy (%)
θ (°)	t_p (ms) - $cos\ \varphi \sim 0.1$		
12	6.96	6.13	12
90	14.16	12.68	10
160	8.85	7.90	11

	Simulations	Experiments	Relative discrepancy (%)
θ (°)	t_p (ms) - $cos\ \varphi \sim 0.9$		
6	5.11	4.67	9
90	4.77	2.53	47
160	6.60	5.64	15

Table 2: Experimental pre-arcing times and equivalent temperature for the two power factors.

	$cos\ \varphi \sim 0.1$		$cos\ \varphi \sim 0.9$	
θ (°)	t_p (ms)	T_{eq} (K)	t_p (ms)	T_{eq} (K)
6.7 - 12.1	6.13	1656	4.67	2433
90	12.68	1766	2.53	1235
160	7.90	1300	6.64	1235

4. DISCUSSION

Table 3 gives the simulated pre-arcing times and the W_J values, during the four stages previously quoted for the three closing angles under $cos\ \varphi \sim 0.1$. The distribution of the Joule energies is quite similar during each corresponding stage for the different closing angles. Indeed, except in the stage 1 and in stage 4 of θ=90° for which the energies represent respectively ~45% and ~35% of the whole dissipated energy; the percentages of the dissipated energies for all the relevant cases are quite similar:

Table 3: Simulated pre-arcing times and W_J during the four stages under $cos\ \varphi \sim 0.1$.

$cos\ \varphi \sim 0.1$		W_J (J)			
θ (°)	Pre-arcing time (ms)	stage 1	stage 2	stage 3	stage 4
12	6.96	4.14	0.62	1.81	4.23
90	14.16	7.39	0.81	2.52	5.73
160	8.85	4.17	0.62	1.77	4.11

- In stage 1 the percentage is ~38% for θ=12° and ~39% for θ=160°,
- In stage 2 the percentage is ~6% for θ=12° and θ=160°, and ~5% for θ=90°,
- In stage 3 the percentage is ~17% for θ=12° and θ=160°, 15% for θ=90°,
- In stage 4 the percentage is ~39% for θ=12° and θ=160°.

Table 4: Simulated pre-arcing times and W_J during the four stages under *cos* $\varphi \sim 0.1$.

cos $\varphi \sim 0.9$		W_J (J)			
θ(°)	Pre-arcing time (ms)	Stage1	Stage 2	Stage 3	Stage 4
6	5.11	3.92	0.58	1.75	4.05
90	4.77	3.78	0.58	1.98	4.14
160	6.60	3.93	0.58	1.72	4.14

The percentages of the dissipated energies for all the relevant cases are quite similar:

- In stage 1 the percentage is ~38% for θ=6°*and* θ= 160°, ~36% forθ=90° ,
- In stage 2 the percentage is ~6% for θ=6°, θ=90°and θ=160°,
- In stage 3 the percentage is ~17% for θ=6° and θ=160°, *19%* for θ=90°,
- In stage 4 the percentage is ~39% for θ=6°, 40% for θ=90° and θ=160°.

Table 4 gives the simulated pre-arcing times and the dissipated energy values, during the four stages previously quoted for the three closing angles under *cos* $\varphi \sim 0.9$.

In simulation and in experiments it is observed that the pre-arcing stage is much longer in the inductive case compared to the resistive case. This observation is made for all the relevant closing angles due to the fact that the prospective current is most important in the resistive case compare to the inductive one.

Both under inductive and resistive case, pre-arcing times obtained by experiments are lower than those obtained in simulations; two main reasons could explain that.

First, previous works [6,9] attributed the uncertainties between simulation and experiment to irregularity found in the notch shape and to the fact that sometimes one or some silica grains are unfortunately introduced in the center of the fuse. Second, the discrepancies observed between simulations and experiments are mainly due the physical state at which the fuse link should disrupt. According to us, mechanical stress must be taken into account and these forces are also responsible of the rupturing of the fuse. Indeed the equivalent temperature value corresponding to measurements, pre-arcing times is observed in most cases at time t_p corresponding to $t_{Tm} < t_p < t_{Tvap}$.

Conclusion

In this study was investigated the simulated and measurement response of a HBC fuse submitted to typical fault currents under *AC* supply. Two key parameters such as the closing angle and the power factor were used to characterize electrical fault test conditions close to the industrial test conditions and required by international standards. The prospective fault was founded to be dependent on such parameters and consequently the pre-arcing time. A resistive power factor gives fault current higher than the inductive power factor, and then the pre-arcing time was founded to be longer in the inductive case compared to the pre-arcing time in the resistive case. The role played by the closing angle in the pre-arcing duration was analyzed and we found that typical closing angle values involve maximum dissipated energy which is interesting for Joule integral prediction. This is very important for industrialist and for standard organizations in prediction of "the current/heat integral'' curves. Good agreements between simulations and experiments were founded by the fact that the mathematical model reproduces easily tested conditions close to industrials. Some discrepancies were observed which could be explained by the fact that the enthalpy dependence of the thermal conductivity found in the literature (calculated and measured) is given up to the temperature of 1900 K, above all data has been fitted. We also did not take into account the volume expansion [13] of density calculation after melting.

The equivalent temperature related to the measured pre-arcing time supposed that disrupting of the fuse is not only due the thermal process. This supposed that other contribution possibly due to mechanical stress is combined to the thermal stress to cause the rupturing of the fuse element before the end of the whole latent heat.

References

[1] A. Wright, P. G. Newberry, Electric Fuses, IEE Power & Energy Series, vol. 49, 3rd edn, London, 2001.
[2] J. W. Gibson, the high-rupturing-capacity cartridge fuse, with special reference to short-circuit performance, Journal of the IEE, vol. 88, January, 2-24, 1941.
[3] J. G. Leach, P. G. Newberry, A. Wright, Analysis of high-rupturing-capacity fuselink prearcing phenomena by a finite-difference method, Proceedings of the IEE, vol. 120, n°9, September, 987-993, 1973.
[4] R. Wilkins and P.M. McEwan, A. C. short-circuit performance of notched fuse elements, Proceedings of the IEE, vol. 122, n°3, March, 289-292, 1975.
[5] C. B. Wheeler, optimum conditions for electrical testing fuses. I Maximization of the prearcing energy, J. Phys. D: Applied Physics, vol. 9, 1809-1816, 1976.
[6] W. Bussière, D. Rochette, G. Velleaud, T. Latchimy, J. L. Gelet, F. Gentils, J. C. Perez-Quesada, T. Rambaud and P. André, Experimental study of HBC fuses working at short and medium pre-arcing times, J. Phys. D: Applied Physics, vol. 41, 2008, 195210.
[7] S. Memiaghe, W. Bussière, D. Rochette, R. Touzani and P. André, pre-arcing times in HBC fuses for high fault currents. Comparison between simulation and experiment, High. Temp. Mater. and Proc., vol. 12, n°3/4, 345-364, 2008.
[8] IEC 60282-1 High Voltage fuses –Part 1: Current-Limiting Fuses, November 1, 2005.
[9] D. Rochette, R.Touzani and W. Bussière, Numerical study of the short pre-arcing time in high breaking capacity fuses via an enthalpy formulation, J. Phys. D: Applied Physics, vol. 40, 2007, 4544-4551.
[10] R.A. Matula, Electrical Resistivity of Copper, Gold, Palladium, and Silver JPCRD 8(4), 1147-1298, 1979.
[11] I. Bahrin, Thermochemical Data of Pure Substances, 3rd ed. in collaboration with G. Platzki, vol. 1. Ag-Kr and vol. 2. La-Zr, VCH Weinheim, Federal Republic of Germany, New York, 1995.
[12] Y.S.Touloukian, R.W. Powell and C.Y. Ho, Thermal conductivity - metallic elements and alloys, Vol. 1 of Thermophysical properties of Matter – the TPRC Data Series, ed. IFI/Plenum New York Washington, 1970.
[13] C. Cagran, B. Wilthan and G. Pottlacher, Enthalpy, heat of fusion and specific electrical resistivity of pure silver, pure copper and the binary Ag-28Cu Alloy, Thermochimica Acta 445, 2006, 104-110.